JOURNAL OF SANDWICH STRUCTURES & MATERIALS

Original Article

Homogenized modeling and micromechanics analysis of thin-walled lattice plate structures for brake discs

Journal of Sandwich Structures & Materials
0(0) 1–38

DOI: 10.1177/1099636218757670
journals.sagepub.com/home/jsm
SAGE

Aminreza Karamoozian[1], Chin An Tan[2] and Liangmo Wang[1]

Abstract

Periodic cellular structures, especially lattice designs, have potential to improve the cooling performance of brake disk system. In this paper, the method of two scales asymptotic homogenization was used to indicate the effective elastic stiffnesses of lattice plates structures. The arbitrary topology of lattice core cells connected to the back and front plates which are made of generally orthotropic materials, due to use in brake disc design. This starts with the derivation of general shell model with consideration of the set of unit cell problems and then making use of the model to determine the analytical equations and calculate the effective elastic properties of lattice plate concerning the connected back and front plates. The analytical and numerical method allows determining the stiffness properties and the internal forces in the trusses and plates of the lattice. Three types of core-based lattice plates, which are pyramidal, X-type and I-type lattices, have been studied. The I-type lattice is characterized here for the first time with particular attention on the role that the cell trusses and plates plays on the stiffness and strength properties. The lattice designs are finite element characterized and compared with the numerical and experimentally validated pyramidal and X-type lattices under identical conditions. The I-type lattice provides 4% higher strength more than the other lattice types with 9% higher truss fraction

[1]Department of Automotive Engineering, School of Mechanical Engineering, Nanjing University of Science and Technology, Nanjing, PR China
[2]Department of Mechanical Engineering, Wayne State University, Detroit, USA

Corresponding author:
Liangmo Wang, Department of Automotive Engineering, Nanjing University of Science and Technology, Nanjing, China.
Email: liangmo@njust.edu.cn

coefficient. Results show that the stiffness and yield strength of the lattices depend upon the stress–strain response of the parent alloy of trusses and plates, the truss mass fraction coefficient, the face carriers thickness and the core elements parameters. The study described here is limited to a linear analysis of lattice properties. Geometric nonlinearities, however, have a considerable impact on the effective behavior of a lattice and will be the subject of future studies.

Keywords
Cellular, thin-walled, lattice, stiffness, brake disc

Introduction

Nowadays, forced convective heat transfer of braking systems is very important. Current ventilated brake discs have the design of Pin–fins or vanes structure which is configured two-dimensionally to the rubbing discs. The design may not be desirable for forced convective heat transfer because of the heat transfer area and limited flow mixing [1,2]. In this situation, researchers motivate to improve the heat dissipation and cooling performance of brakes by novel designs. Accordingly, design and selection of heat dissipation elements for brake discs have great importance. Hydraulically actuated disc brakes with their superior cooling performance are widely known in passenger vehicles [3,4]. Deceleration of vehicle caused by the transformation of kinetic and potential energies into the thermal energy by considering the friction occurs between the brake disc and pads. Hence, overheating of braking components is usually influenced by different frictional heating situations which cause high load braking during repeated high-speed braking or continuous downhill braking. This substantially raises the temperature at the friction interface up to 900 K [5,6].

Overheating in the braking system can cause important issues such as deterioration of friction coefficient [7,8], thermal cracking of components especially brake disc, the efficacy of friction wear [9] and making noise in the braking system [6,7,10]. Therefore, the cooling properties of braking components and contact stiffness of brake disc and pads have an important influence on efficiency and safety of the braking system and substantially for high-performance passenger vehicles is more ostensible. Designing brake disc is very important especially with consideration of effects on decreasing the heat accumulation in brake pads [8]. The majority of generated heat friction is transferred to the brake disc (approximately 90%) concerning the contact stiffness of brake system [11]. The contact stiffness has been influenced by the stiffness of the brake disc, pressure load variation, non-linearity of friction material, etc. Much research has been done on the

load variation, friction material effects and other parameters of the braking system.

A connected network of struts is named lattice, which is made of an array of struts, pin-jointed or rigidly bonded at their connections (Figure 1). Their general purpose is to make strong, light, stiff structures using as little material as possible, which has high energy absorbing and fluid flow properties [12]. The three-dimensional (3D) interconnected lattice structures with void spaces that have high properties for allowing fluid flow through them are more interested and investigated [13]. A comprehensive study has been done on the lattice stiffness, yielding and buckling properties concerning von Mises criterion [14,15]. Studies have been done on the effect of the cell aspect ratios on the stiffness and strength properties [16]. The plastic yielding properties are considered to analyze the in-plane strength and stiffness of some individual lattice cell topologies [17]. Recently, a type of lattice structure was used to the brake disc structure to improve the thermal efficiency of the disc brake and braking system. The new brake disc has revealed that at steady-state tests, in typical operating range of rotating speed (200–1000 r/min), could be provided less pumping capacity than radial vanes. Also, it has provided more complex flow mixing and 1.1 times more heat transfer area caused by the lattice core [18].

By using lattice structure as the brake disc, we should define the stiffness of lattice jointed to the back and front plate of brake disc together as lattice plate [19,20], because changes in each parameter of the lattice plate [21] (thickness of trusses, thickness of back or front plates, etc.) easily changes the contact stiffness. In this paper, we focus on the calculation of the stiffness and critical mechanical properties of lattice structure to use in brake disc design with respect to the new design of lattice (I-type). The comparison with the pyramid and X-type lattices in the mechanical principles have been done to find and investigate which parameters are important in stiffness properties. The results will be used for the vibration and stability analysis of lattice brake disc in future studies.

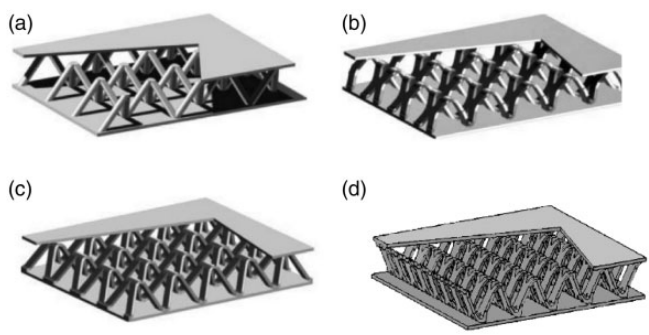

Figure 1. Schematics of some lattice plates with (a) tetrahedral, (b) X-type lattice cores (c) pyramidal and (d) I-type lattice cores.

Homogenized modeling and analysis of lattice to use in brake disc

To use lattice structures in brake disc design, it would be necessary to define the mechanical properties by the homogenized modeling and micro-mechanics properties of the designed structure. Homogenized constants or in other name macroscopic properties are related to variational principles. Primary researches on variational principles and homogenized constants of composites were established in the 1920s–1950s. Outstanding homogenization method has been obtained for homogenized constants of composites with 3D solid-like structure in 1980s [22,23]. The stiffnesses homogenized constants of beams and plates was estimated and determined by derivation of the variational principles for an inhomogeneous of periodic structure plate by using homogenization method, Castigliano and Lagrange principles [24–27]. Kolpakov [28] showed that precise variational principles for homogenized stiffnesses should be obtained from a 3D elasticity problem without any additional hypothesis immediately. Therefore, for a plate at first, we should use the homogenization method and relate the 3D elasticity problem of a thin body to 2D plate strain characteristics.

A lattice structure with individual truss design core is analyzed at two different scales. We considered the lattice structure treated as a homogeneous solid at the macroscopic scale, at the microscopic scale approach. We analyzed the individual structural lattice elements by using the principles of structural mechanics. We can design the lattice structure for supporting the bending loads by lining up the truss topology [29]. Therefore, concerning the alignment of trusses, the axial deformations are subject to consideration [16,30]. In order to calculate the stiffness and critical mechanical properties of the lattice structure concerning use in brake disc design, we compare the new design of lattice (I-type) with the pyramid and X-type lattices in the mechanical principles to define the important stiffness parameters. We have used the unit cell of lattice structures as shown in Figure 1 to define the micro-macro relations of the structure.

Comparatively, the new I-structure has different types of nodes with respect to the pyramidal structure. It has nodes that are constrained between the strut members and also nodes that are brazed between the struts and the faceplates. The braze alloy has added extra weight to the lattice structure, causing about 0.2% increase in relative density [31]. Concerning the length, geometry and cross-sectional area of the lattice strut member and the unit cells shown in Figure 2, the I-type unite cell volume is given by (for pyramidal and X-type structures have been driven in last published papers respectively [18,32])

$$V_U = 4(h + 2\ell\cos\theta)(h + 2\ell\sin\theta)\ell\sin\theta\sin\omega \;\; \sin2\omega \tag{1}$$

where ℓ is the strut length and ω is the inclination angle between the truss member and the base of the unit cell. The total volume of the solid metal within the unit cell

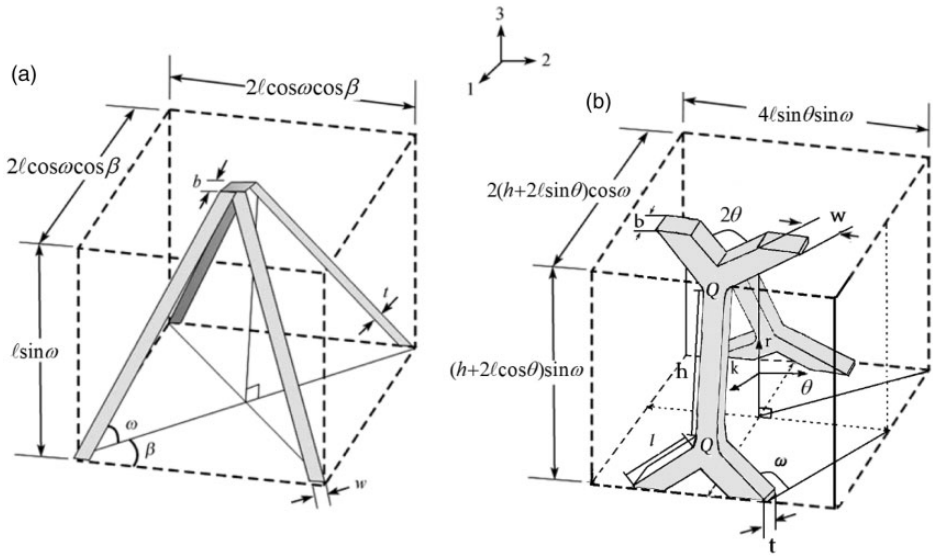

Figure 2. (a) and (b). Schematically the unit cells of periodic pyramidal [13] and I-type lattice truss structures.

is the same for all types of structures. With regard to a rectangular cross-section of width w and thickness for trusses (Figure 2), the total volume of occupied by metal is given by

$$V_T = 4\omega t(h + 2\ell\cos\theta + b) \tag{2}$$

where b is the brazed node width area and node area assumed has a square shape (it should be noted that in ideal lattice structure b is equal to zero). The relative density of lattice structure can be found by dividing the volume of occupied metal to the unit cell volume [14,32,33], so the relative density of I-type lattice cell is given by

$$\overline{\rho} = \frac{V_T}{V_U} = \frac{\left({}^{\omega t}/_{\ell}\right)(h + 2\ell\cos\theta + b)}{(h + 2\ell\cos\theta)(h + 2\ell\sin\theta)\sin\theta\sin\omega\ \sin 2\omega} \tag{3}$$

There is no contribution of the flat nodes (with a width of b) to the stiffness and strength of the lattice truss core structure (shown in Figure 2). On the other hand, stiffness reduction happens when getting away from an ideal lattice structure (where $b = 0$) [14,33]. Accordingly, a truss mass fraction factor η has been introduced, which leads to an expression that separates components of the core

topology into those that directly contribute to the stiffness from those that are applied to achieve robust performance [14,32,33]

$$\eta = \frac{(h + 2\ell\cos\theta)}{(h + 2\ell\cos\theta + b)} \tag{4}$$

The mass truss fraction will extend to the compressive and shear strength of the lattice structure.

We modeled cellular truss structures as an-isotropic continuum medium to analyze the strengths of periodic pyramidal, X-type and I-type lattices having unit cells as in Figure 2.

The homogenized method and problem formulation

The homogenization method is the averaging method for studying partial differential equations with rapidly oscillating coefficients of medium to solve the elastic problems. Rapidly oscillating coefficients are coefficients of partial differential equations of a medium consisting of a basic material. The medium has a lot of small inclusions made of another material which has rapidly changing terms such as the wave equation that has terms of $\mathrm{f(x)} = \sin(\mathrm{x}/\varepsilon), \varepsilon = 1$ with high oscillation. The method is used to evaluate the macroscopic and microscopic elastic characteristics of periodic microstructure which are described by partial differential equations and periodic coefficients [34]. In the present study, the homogenization method is applied to derive the effective elastic stiffnesses of the lattice-cored structural sandwich composite.

A developed research on theoretical and computational methods for describing lattice plates with continuous models have been done by considering the inverse approximation of framework modeled continuum structures [35]. On the other hand, some studies have shown that the problem can describe with respect to the homogenization method and expand a theory for periodic lattice plates by combining the classical methods of the theory of strength and the homogenization method [36].

With considering the periodicity of the cell, the lattice plates are constructed by beams and rods. Periodicity cell issue can be explained by the periodicity theory of beams and rods. Using the strength theory to define the cellular lattice problem has some difficulties. Extraction of equilibrium and kinematic relations and conditions concerning the joint nodes are principal difficulties and issues that have been precisely investigated [26]. We can derive a finite dimensional cell problem for lattice plates of a periodic structure concerning variational principles. Consider an elastic body, like as shown in Figure 3, with a regular distribution of elastic properties. Repeating a periodicity cell Ω_δ is generated the general shell structure, which is determined in the orthogonal curvilinear coordinate system(y_1, y_2, y_3). The main curvature lines of the middle surface coincide with the coordinate lines y_1, y_2 and coordinate line y_3 and is normal to the middle surface $(y_3 = 0)$.

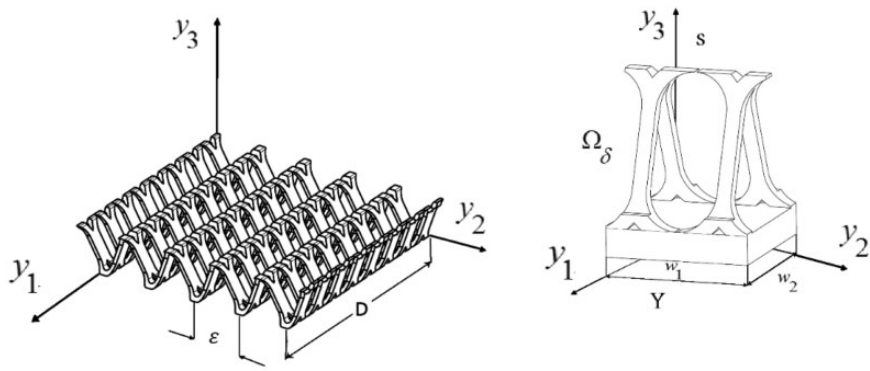

Figure 3. The I-lattice composite layer with representative periodicity cell Ω_δ.

The small parameter δ is dimensionless and characterized the small dimensions of the periodicity cell. It has assumed the thickness of the layer and the dimensions of the unit cell to be small as compared with the dimensions of the structure in whole. The unit cell is defined by the relations $\{\frac{-\delta w_1}{2} < y_1 < \frac{\delta w_1}{2},\ \frac{-\delta w_2}{2} < y_2 < \frac{\delta w_2}{2},\ {y_3}^- < y_3 < {y_3}^+\}$ and ${y_3}^\pm = \pm\frac{\delta}{2} \pm \delta F^\pm(\frac{y_1}{\delta w_1}, \frac{y_2}{\delta w_2})$ (Figure 3). The dimensions of the unit cell in middle surface are δw_1 and δw_2 and the geometry of the upper and lower reinforcing elements defined by the functions $F^\pm$. For this structure the theory of elasticity has the form [28]

$$\begin{aligned} L_\varepsilon u^\varepsilon + F(X) &= 0 \quad \text{in G} \\ u^\varepsilon(x) &= 0 \quad\quad \text{on G} \end{aligned} \tag{5}$$

where

$$L_\varepsilon u = C^\varepsilon_{ijkl}(x) u_{k,l} \tag{6}$$

The occupied region by the composite is defined with G, the initial forces are $F(X)$, the boundary is defined by ∂G, L_ε is the elasticity theory operator, u^ε are the displacements and $C^\varepsilon_{ijkl}(x)$ is a tensor of elastic constants. The elastic body has a periodic structure in coordinates y_1, y_2, y_3 with a period called as the periodicity cell (Figure 3). Parameter ε is related to the characteristic dimension of the periodicity cell of the composite which is clamped on the boundary ∂G. Here the summation is represented over identical indices, with the Latin indices taking on values of 1–3, while the Greek indices take on values of 1 and 2. We can show the material characteristics of the indicated medium described by periodic functions

$$C^\varepsilon_{ijkl}(x) = C_{ijkl}(x/\varepsilon) \tag{7}$$

where the variable x/ε explains the periodic media with rapidly oscillating characteristics. On the other hand, the periodic functions with a periodicity cell Y are

$C_{ijkl}(y)$. To untangle the problem an asymptotic expansion method in the form of special series concerning the oscillating coefficients $C_{ijkl}(y)$ is used [36]

$$u^{\varepsilon} = u^{(0)}(x) + \varepsilon u^{(1)}(x,y) + \ldots = u^{(0)}(x) + \sum_{k=1}^{\infty} \varepsilon^{k} u^{(k)}(x,y) \tag{8}$$

where $y = x/\varepsilon$ is the fast variable and$x$ is slow variable. The Function $u^{(0)}(x)$ is a function only of slow variable x and $u^{(k)}(x,y)$ are periodic in variable y with periodicity cell Y. So, these functions are periodic in x with periodicity cell εY with replacing y for x/ε. We define the solution of elastic body problem (5) by (8) in the form of asymptotic expansion [36]. By using differentiating rule (equation (8)), we can write the elasticity theory operator L_{ε} as

$$L_{\varepsilon}u = \left(\varepsilon^{-2}A_1 + \varepsilon^{-1}A_2 + A_3\right) \sum_{m=0}^{\infty} u^{m} + f(x,y) = 0 \tag{9}$$

where

$$\begin{aligned} A_1 u &= \left[C_{ijkl}(y)u_{k,ly}\right]_{jy} \\ A_2 u &= \left[C_{ijkl}(y)u_{k,ly}\right]_{jx} + \left[C_{ijkl}(y)u_{k,lx}\right]_{jy\,jx} \\ A_3 u &= \left[C_{ijkl}(y)u_{k,lx}\right] \end{aligned} \tag{10}$$

Considering the same order in ε resulted in the infinite sequence of problems, the first three equations are

$$A_1 u^{(0)} = 0 \tag{11}$$

$$A_1 u^{(1)} + A_2 u^{(0)} = 0 \tag{12}$$

$$A_1 u^{(2)} + A_2 u^{(1)} + A_3 u^{(0)} + f(x,y) = 0 \tag{13}$$

Equation (11) is satisfied because of function

$$u^{(0)} = u^{(0)}(x) \tag{14}$$

is independent of variable y. Therefore by considering equation (14), equation (12) will be as follows

$$\left[C_{ijkl}(y)u^{(1)}_{k,ly}\right]_{jy} + \left[C_{ijkl}(y)\right]_{jy} u^{(0)}_{k,ly} = 0 \tag{15}$$

The solution of equation (15) taken out by separating the variables x and y gives

$$u^{(1)}(x,y) = X^{kl}(y)u_{k,lx}(x) + V(x) \tag{16}$$

where $X^{kl}(y)$ demonstrates solution of the problem, the cellular problem for a periodicity cell is

$$\begin{cases} [C_{ijkl}(y)X^{kl}_{k,ly} + [Cijkl(y)]_{,jy} = 0 \ \ in \ \ Y, \\ X^{kl}(y) \ \ is \ \ periodic \ \ in\, y\, with\, periodicity\, cell\, Y \end{cases} \tag{17}$$

This above cellular problem has a periodic solution if the following equality is fulfilled

$$\langle A_2 u^{(1)} + A_3 u^{(0)} \rangle + \langle f \rangle(x) = 0 \tag{18}$$

where $\langle\rangle$ is the average value over the periodicity cell Y.

With acceptance of the rigid joints conditions, we have the problem with the following conditions

1. The forces applied to the elements forming the cellular structure are equal to zero.
2. The rigid-joint conditions are satisfied at the inner nodal points of the cellular structure, and the sum of the forces and sum of the moments at the nodal joints are equal to zero (in other words, the equilibrium conditions are satisfied for the inner nodes).
3. The conditions indicated in item 2 are satisfied at the nodal points of the cellular structure corresponding to the free surface S.

Therefore, from the homogenized equation (18), on account of equation (16), we obtain the homogenized equation (5) for $u^{(0)}(x)$ with the boundary conditions $u^{\varepsilon}(x) = 0$ on ∂G (equation (6)). So, we can extract the equation for the tensor of local elastic constants coefficients $C_{ijkl}(y)$ from equations (16) and (18) as follows

$$C_{ijkl} = \langle C_{ijkl}(y)X^{kl}_{k,ly}(y) + C_{ijkl}(y) \rangle \tag{19}$$

For the problem with initial stresses, consider $\sigma^{\varepsilon}_{ij}$ as the initial stresses which be the result of the usage of surface and mass forces $F(x)$ on the surface G. In this case, the initial stress $\sigma^{\varepsilon}_{ij}$ satisfies the equations as follows [37]

$$\begin{aligned} &\sigma^{\varepsilon}_{ij,j} + F_i(x) = 0 \,\text{in G} \\ &u^{\varepsilon}(x) = 0 \qquad \text{on } \partial G \end{aligned} \tag{20}$$

where

$$\sigma_{ij}^{\varepsilon} = C_{ijkl}^{\varepsilon}(x)u_{k,l}^{\varepsilon} \tag{21}$$

It was proven in [37] that

$$u^{\varepsilon}(x) \to u^{0}(x), \ \ as \ \ \varepsilon \to 0 \tag{22}$$

where $u^{\varepsilon}(x)$ and $u^{0}(x)$ are the solutions of initial and homogenized problems, respectively, and it is also shown in [37]

$$u^{\varepsilon}(x) - \left[u^{0}(x) - \varepsilon X^{kl}(y)u_{k,lx}^{(0)}(x)\right] \to 0, \quad as \ \ \varepsilon \to 0 \tag{23}$$

From equations (21) and (23), the following approximation is extracted for the stress field

$$\sigma_{ij}^{\varepsilon} \approx \left[C_{ijkl}(y)X_{k,ly}^{kl}(y) + C_{ijkl}(y)\right]u_{k,lx}^{(0)}(x) \tag{24}$$

Usually, initial stresses $\sigma_{ij}^{\varepsilon}$ are determined from the solution of the linear elasticity problem, and they are symmetrical concerning indexes i and j. Equation (24) can be written in the form

$$\sigma_{ij}^{\varepsilon} \approx K_{ijkl}\left(\frac{x}{\varepsilon}\right)e_{ij}^{(0)}(x) \tag{25}$$

where

$$K_{ijkl}(y) = C_{ijkl}(y)X_{k,ly}^{kl}(y) + C_{ijkl}(y) \tag{26}$$

is the homogenized stiffnesses of lattice plate and the principal terms in equation (25) are

$$\begin{aligned} e_{ij}(u) &= \frac{1}{2}\left(\frac{\partial u_{i,j}}{\partial y} + \frac{\partial u_{i,j}}{\partial y}\right) \\ e_{ij}^{(0)}(u) &= \frac{1}{2}\left(u_{i,j}^{(0)} + u_{j,i}^{(0)}\right) \end{aligned} \tag{27}$$

In the corresponding expansions for the components of the stress tensor over the small parameter δ, the relationships that determine the local structure stress

field has been demonstrated in Kalamkarov and Georgiades and is

$$\sigma_{ij}^{\varepsilon} \approx b_{ijkl}^{kl}\left(\frac{x}{\varepsilon}\right)e_{ij}(u) + \delta b_{ijkl}^{*kl}\tau_{kl} \tag{28}$$

Strain functions $e_{11} = e_1,\ e_{22} = e_2,\ e_{12} = e_{21} = e/2$ express the shearing and tensile strains in the middle surface; $\tau_{11} = T_{11},\ \tau_{22} = T_2\ ,\ \tau_{12} = \tau_{21} = \tau$ specify the torsional and flexural torsional strains of the middle surface. We used the following definitions according to equation (28) [38]

$$\begin{aligned} b_{ij}^{kl} &= C_{ijkl}(y)\frac{1}{w_l}\frac{\partial U_k^{kl}}{\partial y_1} + C_{ijk3}(y)\frac{\partial U_k^{kl}}{\partial y_3} + C_{ijkl} \\ b_{ij}^{*kl} &= C_{ijkl}(y)\frac{1}{w_l}\frac{\partial V_k^{kl}}{\partial y_1} + C_{ijk3}(y)\frac{\partial V_k^{kl}}{\partial y_3} + y_3 C_{ijkl} \end{aligned} \tag{29}$$

The functions U_k^{kl} and V_k^{kl} depend on y_1, y_2 and y_3. By consideration of y_1 and y_2, the periodic solutions with respect to the periods of A_1 and A_2 on the periodicity cell Ω_δ of the following local problems are defined as

$$\begin{cases} \dfrac{1}{w_1}\dfrac{\partial}{\partial y_l}b_{il}^{kl} + \dfrac{\partial}{\partial y_3}b_{i3}^{kl} = 0 \\ \left(\dfrac{1}{w_1}b_{il}^{kl}N_l^{\pm} + b_{i3}^{kl}N_l^{\pm}\right)|_{y_3 = y_3^{\pm}} = 0 \end{cases} \tag{30}$$

And

$$\begin{cases} \dfrac{1}{w_1}\dfrac{\partial}{\partial y_l}b_{il}^{*kl} + \dfrac{\partial}{\partial y_3}b_{i3}^{*kl} = 0 \\ \left(\dfrac{1}{w_1}b_{il}^{*kl}N_l^{\pm} + b_{i3}^{*kl}N_l^{\pm}\right)|_{y_3 = y_3^{\pm}} = 0 \end{cases} \tag{31}$$

where the component vectors normal to the surface y_3 are indicated by $N_i^{\pm}$. Equations (30), (31) and (29), respectively, indicate the problems which called the unit-cell local problems for the thin inhomogeneous shell structure and are shown in Figure 3. So, we have attained the homogenized periodicity cell local functions U_k^{kl} and V_k^{kl}, which characterize, in turn, the coefficients b_{il}^{kl} and b_{il}^{*kl} in equation (28) and are periodic in y_1 and y_2. These local functions are homogenized because they include only the derivatives according to rapid variables y_1, y_2 and y_3 and help us in obtaining the first term in the stress function σ_{ij}^1. It should be noted that, unlike the unit-cell problems of classical homogenization schemes, those set by equations (30) and (31) depend on the boundary conditions on y_3 rather than on

periodicity in the y_3-direction. The stiffnesses can be determine with respect to equations (24), (26) and (28) as follows [28]

$$K_{ijkl}^{\nu+\mu}(y) = \left\langle [(-1)^{\nu} y_3^{\nu} b_{ij}^{kl}(y) + b_{ij}^{*kl}(y)][(-1)^{\mu} y_3^{\mu}] \right\rangle \tag{32}$$

where superscripts μ and ν take values 0, 1. Equation (32) gives the bending stiffnesses K_{ijkl}^{2} when $\mu = \nu = 1$ the coupling and out-of-plane stiffnesses K_{ijkl}^{1} when $\mu + \nu = 1$ and the in-plane stiffnesses K_{ijkl}^{0} when $\mu = \nu = 0$ [28].

Homogenization of unit-cell problem

For homogenization of unit-cell, the presence of discontinued surfaces along the shell structure should be considered [38], and therefore the following continuity conditions added to the unit-cell problems in equations (30) and (31)

$$\begin{cases} [U_k^{kl}] = 0, & \left[\frac{n_l}{w_l} b_{il}^{kl} + n_3 b_{i3}^{kl}\right] = 0 \\ [V_k^{kl}] = 0, & \left[\frac{n_l}{w_l} b_{il}^{*kl} + n_3 b_{i3}^{*kl}\right] = 0 \end{cases} \tag{33}$$

where n_i is the component normal to the discontinuity surface. Local problems of equation (29) have single solutions accurate to the constant terms b_{il}^{kl} and b_{il}^{*kl}. We can define the averaging over the volume of the periodicity cell. So by averaging relationships in equation (28) over the unit cell volume, we obtain $(r = 0, 1)$

$$\langle y_3{}^r \sigma_{ij} \rangle = \langle y_3{}^r b_{il}^{kl} \rangle e_{kl} + \delta \langle y_3{}^r b_{il}^{*kl} \rangle \tau_{kl} \tag{34}$$

Equation (34) indicates the relationship between the averaged shell status and the effective elastic characteristics indicated by the coefficients of this relationship. According to equations (28) to (33), in arriving at a relationship equation (34), the following has been illustrated

$$\begin{gathered} \langle y_3{}^r b_{i3}^{kl} \rangle = \langle y_3{}^r b_{i3}^{*kl} \rangle = 0 \\ \langle b_{il}^{kl} \rangle = \langle b_{kl}^{il} \rangle, \ \langle y_3 b_{il}^{*kl} \rangle = \langle y_3 b_{kl}^{*il} \rangle, \ \langle b_{il}^{kl} \rangle = \langle b_{kl}^{*il} \rangle \end{gathered} \tag{35}$$

The symmetry of the matrices consist of the coefficients of the equations of averaged shell status created by equations (35). It should be mentioned that, as illustrated by Kalamkarov [24], in the situation that we have uniform material and constant shell thickness ($y_3 \in (\frac{-1}{2}, \frac{1}{2})$) this average plate model brings down the relationships taken from the anisotropic plates theory of the elasticity and gives

the following relations, which are valid for the linear forces, the bending and torsional moments

$$\begin{aligned} N_1 = \delta\langle\sigma_{11}\rangle, N_2 = \delta\langle\sigma_{22}\rangle, N_{12} = \delta\langle\sigma_{12}\rangle, \\ M_1 = \delta^2\langle y_3\sigma_{11}\rangle, M_2 = \delta^2\langle y_3\sigma_{22}\rangle, M_{12} = \delta^2\langle\sigma_{12}\rangle \end{aligned} \tag{36}$$

In brief, the illustration in the above model shows that the local problems at equations (30) and (31) are defined by the structure of the composite plate unit-cell completely and are entirely independent of the global boundary value problem formulation, set in equation (21).

Problem formulation for I lattice

Consider a thin elastic body set up with periodic structure and has a repetition of small dimensions of periodicity cell εY in the Oy_1y_2 plane (Figure 3). For $\varepsilon \to 0$, the 3D body tightens the 2D domain Y at Oy_1y_2 plane. The $C_{ijkl}(\frac{x}{\varepsilon})$ is considered as the tensor of local elastic constants of the body, where $C_{ijkl}(y)$ are periodic functions concerning $(y_1, y_2) \in S$. A two-scale expansion is considered, and S is the projection of Y on the Oy_1y_2 plane. It is assumed that the local elastic constants satisfy the following conditions [26,37]

$$\begin{cases} |C_{ijkl}(y)| < M \quad for\, every\, y \in S \\ C_{ijkl}(y)e_{ij}e_{kl} > m|e_{ij}|^2 \quad for\, every \;\; y \in YT\, and\, e_{ij} = e_{ji} \end{cases} \tag{37}$$

where $0 < m$, $M < \infty$ do not depend on $y \in$ Y and $e_{ij} = e_{ji}$.

The lattice plate stiffness can be calculated by solving the cellular problem and define the effective characteristics that appear in the elasticity relations involving the problem in section the homogenized method and problem formulation which were proposed and verified by Kalamkarov and Kolpakov [26,28,37], so with respect to this case the cellular problem has the form

$$\begin{cases} [C_{ijkl}(y)X^{kl}_{k,ly} + (-1)^{\nu}y_3^{\nu}c_{ijkl}(y)]_{,j} = 0 \;\; in \;\; Y, \\ [C_{ijkl}(y)X^{kl}_{k,ly} + (-1)^{\nu}y_3^{\nu}c_{ijkl}(y)]n_j = 0 \;\; on \;\; S, \\ X^{kl}_{k,ly}(y) is \;\; periodic \;\; in \;\; y_1, y_2 \;\; with \;\; periodicity \\ \qquad\qquad cell \;\; Y \\ \qquad\qquad (\nu = 0, 1) \end{cases} \tag{38}$$

where n_j is the normal to the free surface S of domain Y (Figure 4). Greek indexes take values 1, 2, and superscripts ν, μ take values 0, 1. Also $X^{\nu kl}(y)$ is the solution

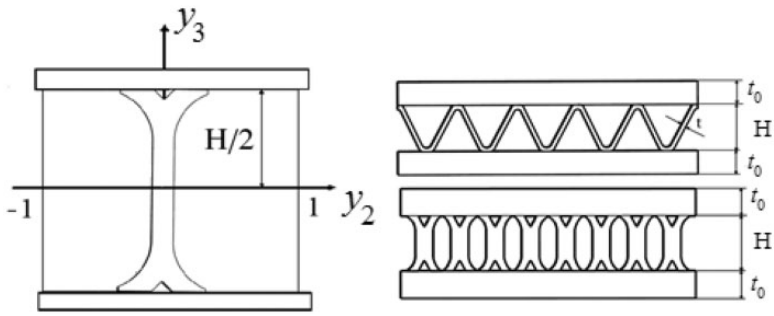

Figure 4. Lattice beam with I-shaped periodicity cell.

of cellular problem. We are able to determine the homogenized characteristics by solving the cellular problem, where ν, μ takes 0, 1; $k\ , l = \ 1, 2$. The stiffnesses are determined by solving the cellular problem for lattice plate (equation (28)) as in section 2.1 and gives the formula as follows

$$K_{ijkl}^{\nu+\mu} = \left\langle C_{ijkl}(y)[X_{k,l}^{\nu kl}(y) + (-1)^{\nu} y_3^{\nu}][(-1)^{\mu} y_3^{\mu}] \right\rangle \tag{39}$$

And by substituting equation (30) we obtain

$$K_{ijkl}^{\nu+\mu}(y) = \left\langle [(-1)^{\nu} y_3^{\nu} b_{ij}^{kl}(y) + b_{ij}^{*kl}(y)] [(-1)^{\mu} y_3^{\mu}] \right\rangle \tag{40}$$

Concerning the theory of plates and shells, in order to define the effective characteristics that appear in the elasticity relations, as well as illustrated in the current solution of local problems in equations (29)–(31), an approximated method was proposed and verified by Kolpakov [39]. With the consideration that the governed basic mechanics equations related to the flexural and membrane rigidities can be simplified by using the typically sandwich structures assumptions, the assumption that the thickness of each of the unit-cell elements is small in comparison with the other two dimensions is used to define the approximate analytical solution of the local problems equations (29)–(31) for a unit-cell of the relevant kind of geometry. The carrier faces are set out symmetrically and similarly with respect to the center of the sandwich structure. The generally orthotropic material is used to make both carrier plates and lattice core of this sandwich composite structure. In order to simplify the computations, we limit our attention to the situation when both coefficients defined for characterizing the quadratic form of the shell middle surface are unity. As shown in Figure 4, for the case of the structure in this research and existence of rotated elements, we use the coordinate systems that are at an angle with respect to the principal coordinate systems. Subsequently, the rotated elements will show monoclinic-like behavior in spite

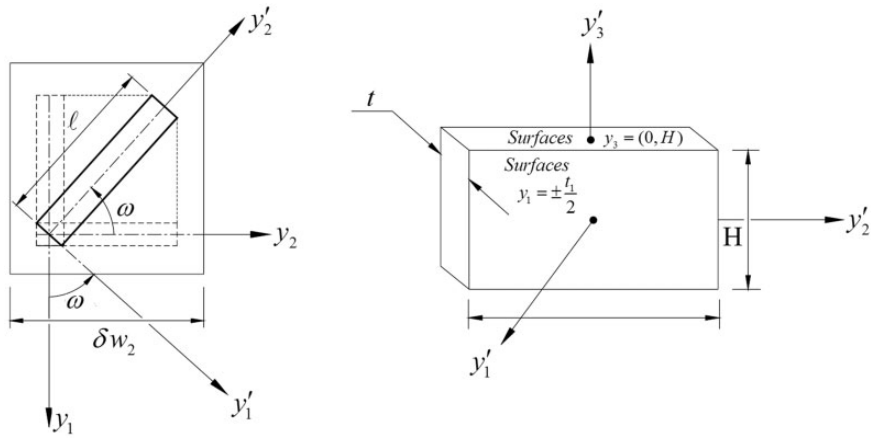

Figure 5. Rotated cellular core and specification of boundary conditions on surfaces $y_1' = \mp^{t_1}/_2$ and $y_3' = (0, H)$[38].

of the sandwich structure made of the orthotropic material, if the principal material coordinates not related to them. As shown in the periodicity unit cell Figure 3, at first we simplify the unit-cell problem to the unit cell with only a single element rotated at an arbitrary angle ω with respect to the y_2' axis. This rotated unit-cell is shown in Figure 5.

Therefore, with finding the solution for this rotated unit-cell, we define a simple superposition that will extend to compute the solution for the complete lattice core concerning angle ω for participating elements $\Omega_1$to Ω_{12} (Figure 6).

To solve the problem for I type lattice, we consider reducing the order of the associated differential equations. Therefore, assume that the element is located along the coordinate axes y_2', this alignment making the problem independent of y_2'. The functions U_k^{kl} and V_k^{kl} will then depend on the variables y_1' and y_3', and the local problems of the group b_{il}^{kl} and b_{il}^{*kl} $(kl = 11, 22, 12)$ simplify to the definition of the functions $U_2^{kl}(y_1', y_3')$, $U_3^{kl}(y_1', y_3')$, $(kl = 11, 22)$ and $U_3^{kl}(y_1', y_3')$ from the system of equations obtained by

$$\frac{\cos\omega}{w_1}\frac{\partial \tau_{i1}^{kl}}{\partial y_1'} + \frac{\sin\omega}{w_2}\frac{\partial \tau_{i2}^{kl}}{\partial y_1'} + \frac{\partial \tau_{i3}^{kl}}{\partial y_3'} = 0 \tag{41}$$

Concerning the appropriate conditions on the outer surfaces (Figure 5) $y_1' = \mp {}^{t_1}/_2$ and $y_3' = (0, \mathrm{H})$, we have

$$\begin{cases} t_1^{11} = t_1^{22} = t_2^{11} = t_{22}^2 = t_1^{12} = t_2^{12} = 0 \\ t_3^{11} = \tau_{33}^{11} = -c_{13}, \quad t_3^{22} = \tau_{33}^{22} = -c_{23}, \quad t_3^{12} = \tau_{33}^{12} = -c_{36} \end{cases} \tag{42}$$

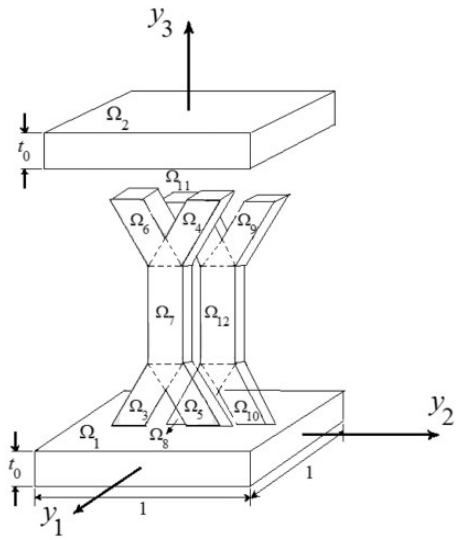

Figure 6. A three-layered sandwich shell reinforced with I-lattice filler.

And according to the boundary conditions above, the following system of equations are obtained

$$\begin{cases} t_3^{11} = \left({}^{\cos\omega}/_{w_1}\right)\tau_{33}^{11} + \left({}^{\sin\omega}/_{w_2}\right)\tau_{23}^{11} = 0 \\ t_3^{22} = \left({}^{\cos\omega}/_{w_1}\right)\tau_{33}^{22} + \left({}^{\sin\omega}/_{w_2}\right)\tau_{23}^{22} = 0 \\ t_3^{12} = \left({}^{\cos\omega}/_{w_1}\right)\tau_{33}^{12} + \left({}^{\sin\omega}/_{w_2}\right)\tau_{23}^{12} = 0 \end{cases} \tag{43}$$

where

$$\begin{cases} \tau_{33}^{kl} = \left(\dfrac{c_{13}\cos\omega}{w_1} + \dfrac{c_{36}\cos\omega}{w_2}\right)\dfrac{\partial V_1^{kl}}{\partial y_1'} + \left(\dfrac{c_{36}\cos\omega}{w_1} + \dfrac{c_{23}\cos\omega}{w_2}\right)\dfrac{\partial V_2^{kl}}{\partial y_1'} + c_{33}\dfrac{\partial V_3^{kl}}{\partial y_3'} \\ \tau_{23}^{kl} = c_{45}\dfrac{\partial V_1^{kl}}{\partial y_3'} + c_{44}\dfrac{\partial V_2^{kl}}{\partial y_3'} + \left(\dfrac{c_{45}\cos\omega}{w_1} + \dfrac{c_{44}\cos\omega}{w_2}\right)\dfrac{\partial V_3^{kl}}{\partial y_1'} \\ \tau_{13}^{kl} = c_{55}\dfrac{\partial V_1^{kl}}{\partial y_3'} + c_{45}\dfrac{\partial V_2^{kl}}{\partial y_3'} + \left(\dfrac{c_{55}\cos\omega}{w_1} + \dfrac{c_{45}\cos\omega}{w_2}\right)\dfrac{\partial V_3^{kl}}{\partial y_1'} \end{cases} \tag{44}$$

So the solution of the group b_{ij}^{kl} local problems having been determined, we continue to find out the following functions

$$b_{11}=\frac{1}{A}\begin{cases} b_{11}^{11}=\dfrac{\sin^4\omega}{w_2^4}c_{66}\left(-{c_{13}}^2c_{22}-c_{11}{c_{23}}^2-{c_{12}}^2c_{33}+c_{11}c_{22}c_{33}+2c_{12}c_{13}c_{23}\right) \\ b_{22}^{11}=\dfrac{\cos^2\omega\sin^2\omega}{w_1^2w_2^2}c_{66}\left(-{c_{13}}^2c_{22}-c_{11}{c_{23}}^2-{c_{12}}^2c_{33}+c_{11}c_{22}c_{33}+2c_{12}c_{13}c_{23}\right) \\ b_{33}^{11}=b_{23}^{11}=b_{13}^{11}=0 \\ b_{12}^{11}=\dfrac{\cos\ \omega\sin^3\omega}{w_1w_2^3}c_{66}\left(-{c_{13}}^2c_{22}-c_{11}{c_{23}}^2-{c_{12}}^2c_{33}+c_{11}c_{22}c_{33}+2c_{12}c_{13}c_{23}\right) \end{cases}$$

$$b_{22}=\frac{1}{A}\begin{cases} b_{11}^{22}=\dfrac{\cos^2\omega\sin^2\omega}{w_1^2w_2^2}c_{66}\left(-{c_{13}}^2c_{22}-c_{11}{c_{23}}^2-{c_{12}}^2c_{33}+c_{11}c_{22}c_{33}+2c_{12}c_{13}c_{23}\right) \\ b_{22}^{22}=\dfrac{\cos^4\omega}{w_1^4}c_{66}\left(-{c_{13}}^2c_{22}-c_{11}{c_{23}}^2-{c_{12}}^2c_{33}+c_{11}c_{22}c_{33}+2c_{12}c_{13}c_{23}\right) \\ b_{33}^{22}=b_{23}^{22}=b_{13}^{22}=0 \\ b_{12}^{22}=-\dfrac{\sin\ \omega\cos^3\omega}{w_2w_1^3}c_{66}\left(-{c_{13}}^2c_{22}-c_{11}{c_{23}}^2-{c_{12}}^2c_{33}+c_{11}c_{22}c_{33}+2c_{12}c_{13}c_{23}\right) \end{cases}$$

$$b_{12}=\frac{1}{A}\begin{cases} b_{11}^{12}=-\dfrac{\cos\omega\sin^3\omega}{w_1w_2^3}c_{66}\left(-{c_{13}}^2c_{22}-c_{11}{c_{23}}^2-{c_{12}}^2c_{33}+c_{11}c_{22}c_{33}+2c_{12}c_{13}c_{23}\right) \\ b_{22}^{12}=-\dfrac{\cos^3\omega\sin\omega}{w_2w_1^3}c_{66}\left(-{c_{13}}^2c_{22}-c_{11}{c_{23}}^2-{c_{12}}^2c_{33}+c_{11}c_{22}c_{33}+2c_{12}c_{13}c_{23}\right) \\ b_{33}^{12}=b_{23}^{12}=b_{13}^{12}=0 \\ b_{12}^{12}=\dfrac{\sin^2\omega\cos^2\omega}{w_1^2w_2^2}c_{66}\left(-{c_{13}}^2c_{22}-c_{11}{c_{23}}^2-{c_{12}}^2c_{33}+c_{11}c_{22}c_{33}+2c_{12}c_{13}c_{23}\right) \end{cases} \tag{45}$$

where

$$A = \left(\frac{\cos^{12}\omega}{w_1^4} + \frac{\sin^{12}\omega}{w_2^4}\right) c_{66}(c_{11}c_{22} - {c_{23}}^2) \tag{46}$$

We do in the similar way for the group of b_{il}^{*kl} $(kl = 11, 22, 12)$ local problems, the 2D forms of equations with the appropriate conditions on surfaces (Figure 6) $y_1' = \mp^{t_1}/_2$ and $y_3' = (0, \mathrm{H})$, obtained as follows

$$\frac{\cos\omega}{w_1}\frac{\partial \tau_{i1}^{kl}}{\partial y_1'} + \frac{\sin\omega}{w_2}\frac{\partial \tau_{i2}^{kl}}{\partial y_1'} + \frac{\partial \tau_{i3}^{kl}}{\partial y_3'} = -c_{i3kl} \tag{47}$$

$$\begin{cases} \bar{t}_1^{11} = \bar{t}_1^{22} = \bar{t}_2^{11} = \bar{t}_{22}^{2} = \bar{t}_1^{12} = \bar{t}_2^{12} = 0 \\ \bar{t}_3^{11} = \bar{\tau}_{33}^{11} = -y_3 c_{13}, \quad \bar{t}_3^{22} = \bar{\tau}_{33}^{22} = -y_3 c_{23}, \quad \bar{t}_3^{12} = \bar{\tau}_{33}^{12} = -y_3 c_{36} \end{cases} \tag{48}$$

Where the following system of equations is

$$\begin{cases} \bar{\tau}_{33}^{kl} = \left(\frac{c_{13}\cos\omega}{w_1} + \frac{c_{36}\cos\omega}{w_2}\right)\frac{\partial V_1^{kl}}{\partial y_1'} + \left(\frac{c_{36}\cos\omega}{w_1} + \frac{c_{23}\cos\omega}{w_2}\right)\frac{\partial V_2^{kl}}{\partial y_1'} + c_{33}\frac{\partial V_3^{kl}}{\partial y_3'} \\ \bar{\tau}_{23}^{kl} = c_{45}\frac{\partial V_1^{kl}}{\partial y_3'} + c_{44}\frac{\partial V_2^{kl}}{\partial y_3'} + \left(\frac{c_{45}\cos\omega}{w_1} + \frac{c_{44}\cos\omega}{w_2}\right)\frac{\partial V_3^{kl}}{\partial y_1'} \\ \bar{\tau}_{13}^{kl} = c_{55}\frac{\partial V_1^{kl}}{\partial y_3'} + c_{45}\frac{\partial V_2^{kl}}{\partial y_3'} + \left(\frac{c_{55}\cos\omega}{w_1} + \frac{c_{45}\cos\omega}{w_2}\right)\frac{\partial V_3^{kl}}{\partial y_1'} \end{cases} \tag{49}$$

The solution of the group b_{ij}^{kl} local problems having been found

$$b_{11}^{*} = \frac{y_3}{B}\begin{cases} b_{11}^{*11} = w_1^3 \sin^{11}\omega(-{c_{13}}^2 c_{22} - c_{11}{c_{23}}^2 - {c_{12}}^2 c_{33} + c_{11}c_{22}c_{33} + 2c_{12}c_{13}c_{23}) \\ +2w_1 w_2^2 \cos^{10}\omega\sin\omega c_{66}(c_{11}c_{33} - {c_{13}}^2) \\ b_{22}^{*11} = 2w_1 w_2^{10}\cos^{10}\omega c_{66}(c_{12}c_{33} - c_{13}c_{23}) \\ b_{33}^{*22} = b_{23}^{*22} = b_{13}^{*22} = 0 \\ b_{12}^{*11} = -w_1^3 \cos\ \omega\sin^{10}\omega(-{c_{13}}^2 c_{22} - c_{11}{c_{23}}^2 - {c_{12}}^2 c_{33} + c_{11}c_{22}c_{33} + 2c_{12}c_{13}c_{23}) \\ +2w_1^3 \cos\ \omega\sin^{10}\omega c_{66}(c_{11}c_{33} - {c_{13}}^2 + c_{12}c_{33} - c_{13}c_{23}) \\ -2w_1^2 w_1 \cos\ \omega\sin^{10}\omega c_{66}(c_{12}c_{33} - c_{13}c_{23}) \end{cases}$$

$$b_{22}^{*}=\frac{y_3}{B}\begin{cases} b_{11}^{*22}=2w_1^2w_1\cos\ \theta\sin^{10}\theta c_{66}(c_{12}c_{33}-c_{13}c_{23}) \\ b_{11}^{*22}=2w_1^2w_1\cos\ \theta\sin^{10}\theta c_{66}(c_{12}c_{33}-c_{13}c_{23}) \\ b_{33}^{*22}=b_{23}^{*22}=b_{13}^{*22}=0 \\ b_{12}^{*11}=-w_1^3\sin\ \omega\cos^{10}\omega(-{c_{13}}^2c_{22}-c_{11}{c_{23}}^2-{c_{12}}^2c_{33}+c_{11}c_{22}c_{33}+2c_{12}c_{13}c_{23}) \\ +2w_2^3\sin\ \omega\cos^{10}\omega c_{66}(c_{11}c_{33}-{c_{13}}^2+c_{12}c_{33}-c_{13}c_{23}) \\ -2w_1w_2^2\sin\ \omega\cos^{10}\omega c_{66}(c_{12}c_{33}-c_{13}c_{23}) \end{cases}$$

$$b_{12}^{*}=\frac{y_3}{B}\begin{cases} b_{11}^{*22}=-w_2^2\cos^{11}\omega c_{66}(c_{12}c_{33}-{c_{13}}^2)+w_1^2w_1\cos\ \omega\sin^{10}\omega c_{66}(c_{12}c_{33}-c_{13}c_{23}) \\ +2w_1^3\sin^{10}\omega\cos\ \omega c_{66}(c_{11}c_{33}-{c_{13}}^2) \\ b_{22}^{*22}=-w_2^3\cos^{11}\omega c_{66}(c_{12}c_{33}-c_{13}c_{23})+w_1^2w_2\sin^{10}\omega\cos\ \omega c_{66}(c_{11}c_{33}-{c_{13}}^2) \\ b_{33}^{*22}=b_{23}^{*22}=b_{13}^{*22}=0 \\ b_{12}^{*11}=w_1^3\sin^{11}\omega c_{66}(c_{11}c_{33}-{c_{13}}^2)+2w_1^2w_2\cos^{10}\omega\sin\ \omega c_{66}(c_{12}c_{33}-c_{13}c_{23}) \\ -2w_2^3\sin\ \omega\cos^{10}\omega c_{66}(c_{11}c_{33}-{c_{13}}^2) \end{cases} \tag{50}$$

where

$$B=w_1^3\sin^7\omega c_{66}(c_{11}c_{22}-{c_{23}}^2)+w_2^3\cos^6\sin\omega\left(c_{11}c_{33}-{c_{13}}^2+c_{12}c_{33}-2c_{13}c_{23}\right) +w_2^2\cos^6\sin\omega(c_{12}c_{33}-c_{13}c_{23}+2c_{33}c_{66}) \tag{51}$$

Now to obtain the solution for the whole lattice core, we can replace these b_{il}^{kl} and b_{il}^{*kl} functions in equations (45) and (50) to proper angle ω for each of the elements Ω_3 to Ω_{12}. In this regard, we also need to consider the top and bottom face carriers for determination of the effective elastic characteristics of the complete sandwich structure.

Unit-cell with considering the top and down carrier plates

We apply a similar way which has been used for the lattice core structure for the face carriers and consider that the faces are made of generally orthotropic material. In such a way, we start by defining U_k^{kl} and V_k^{kl} functions and consequently bring

out the solution of the local problem for the group b_{il}^{kl} and group b_{il}^{*kl} functions that properly show the material orthotropic elastic behavior. As it can be observed in Figure 6, a solution will be found for the problem concerning the boundary conditions on surfaces $y_1 = \pm\frac{1}{2}$, $y_2 = \pm\frac{1}{2}$, $y_3 = \mp {}^{t_0}/_2$ and defining the local unit-cell problems in equation (31), also it is a necessity that the surface boundary conditions satisfy $y_3 = \mp {}^{t_0}/_2$, we obtain

$$\frac{\cos\omega}{w_1}\frac{\partial\tau_{i1}^{kl}}{\partial y_1} + \frac{\sin\omega}{w_2}\frac{\partial\tau_{i2}^{kl}}{\partial y_1} + \frac{\partial\tau_{i3}^{kl}}{\partial y_3} = 0 \tag{52}$$

$$\tau_{13}^{kl} = \tau_{23}^{kl} = 0, \qquad \tau_{33}^{11} = -c_{13}, \qquad \tau_{33}^{22} = -c_{23}, \quad \tau_{33}^{22} = 0 \tag{53}$$

Where the local unit-cell problems in equation (31) gives a form

$$\tau_{33}^{kl} = \left(\frac{1}{y_1}\right)c_{13}\frac{\partial U_1^{kl}}{\partial y_1} + \left(\frac{1}{y_2}\right)c_{23}\frac{\partial U_2^{kl}}{\partial y_1} + c_{33}\frac{\partial U_3^{kl}}{\partial y_3} \tag{54}$$

The solution of the group b_{il}^{kl} local problems having been determined, we define the following functions

$$b_{11} = \begin{cases} b_{11}^{11} = c_{11} - \dfrac{{c_{13}}^2}{c_{33}} \\ b_{22}^{11} = c_{12} - \dfrac{c_{23}c_{13}}{c_{33}} \\ b_{33}^{11} = b_{23}^{11} = b_{13}^{11} = b_{12}^{11} = 0 \end{cases}$$

$$b_{22} = \begin{cases} b_{11}^{22} = c_{12} - \dfrac{c_{23}c_{13}}{c_{33}} \\ b_{22}^{11} = c_{22} - \dfrac{{c_{23}}^2}{c_{33}} \\ b_{33}^{22} = b_{23}^{22} = b_{13}^{22} = b_{12}^{22} = 0 \end{cases}$$

$$b_{12} = \begin{cases} b_{11}^{12} = b_{22}^{12} = b_{33}^{12} = b_{23}^{12} = b_{13}^{12} = 0 \\ b_{11}^{12} = c_{66} \end{cases} \tag{55}$$

We define and calculate the group of b_{il}^{*kl} local problems in a similar situation which was done for b_{il}^{kl} from the governing unit-cell problem equations (30), (31) and the corresponding surface boundary conditions. The outcomes are given as

$$\frac{\cos\omega}{w_1}\frac{\partial\tau_{i1}^{kl}}{\partial y_1}+\frac{\sin\omega}{w_2}\frac{\partial\tau_{i2}^{kl}}{\partial y_1}+\frac{\partial\tau_{i3}^{kl}}{\partial y_3}=-c_{i3kl} \tag{56}$$

$$\bar{\tau}_{33}^{kl}=\left(\frac{1}{y_1}\right)c_{13}\frac{\partial V_1^{kl}}{\partial y_1}+\left(\frac{1}{y_2}\right)c_{23}\frac{\partial V_2^{kl}}{\partial y_1}+c_{33}\frac{\partial V_3^{kl}}{\partial y_3} \tag{57}$$

with

$$\bar{\tau}_{13}^{kl}=\bar{\tau}_{23}^{kl}=0,\quad \bar{\tau}_{33}^{11}=-y_3c_{13},\quad \bar{\tau}_{33}^{22}=-y_3c_{23},\quad \bar{\tau}_{33}^{22}=0 \tag{58}$$

So the solution of the group b_{il}^{*kl} local problems having been determined, we continue to find out the following functions

$$b_{11}^{*}=y_3\begin{cases} b_{11}^{11}=c_{11}-\dfrac{{c_{13}}^2}{c_{33}} \\ b_{22}^{11}=c_{12}-\dfrac{c_{23}c_{13}}{c_{33}} \\ b_{33}^{11}=b_{23}^{11}=b_{13}^{11}=b_{12}^{11}=0 \end{cases}$$

$$b_{22}^{*}=y_3\begin{cases} b_{11}^{11}=c_{11}-\dfrac{{c_{13}}^2}{c_{33}} \\ b_{22}^{11}=c_{12}-\dfrac{c_{23}c_{13}}{c_{33}} \\ b_{33}^{11}=b_{23}^{11}=b_{13}^{11}=b_{12}^{11}=0 \end{cases}$$

$$b_{12}^{*}=y_3\begin{cases} b_{11}^{12}=b_{22}^{12}=b_{33}^{12}=b_{23}^{12}=b_{13}^{12}=0 \\ b_{11}^{12}=c_{66} \end{cases} \tag{59}$$

We relate the off-axis coefficient of C_{ijkl} with the principal material coefficients $C_{ijkl}^{(m)}$ by the fourth-order tensor of transformation equation. Afterward, the

principal material coefficients $C_{ijkl}^{(m)}$ can be described by the material constants E, G and v[40]. So, for the effective elastic characteristics of I lattice which are included in the equation of state (34) and are different from zero (with respect to relationships equation (35)), we find

$$
\begin{aligned}
b_{11}^{11} &= \frac{2Et_0}{1-v} + \frac{Ev(h+2\ell\ \cos\theta)\sin\omega)t}{vw} \\
b_{22}^{22} &= \frac{2E_0t_0}{1-v} + \frac{E_0v(h+2\ell\ \cos\theta)\sin\omega)t}{w} \\
b_{22}^{11} = b_{11}^{22} &= \frac{2vEt_0}{1-v} + \frac{Ev(h+2\ell\ \cos\theta)\sin\omega)t}{vw} \\
b_{12}^{12} &= 2Gt_0 + \frac{E_0(h+2\ell\ \cos\theta)\sin\omega)t}{w} \\
y_3b_{11}^{*11} &= \frac{2Et_0}{1-v}\left(\frac{3(h+2\ell\ \cos\theta)\sin\omega)^2}{4} + \frac{3(h+2\ell\ \cos\theta)\sin\omega)}{2} + {t_0}^2\right) \\
&\quad + \frac{E(h+2\ell\ \cos\theta)\sin\omega)^3t}{vw} \\
y_3b_{22}^{*22} &= \frac{2Et_0}{1-v}\left(\frac{3(h+2\ell\ \cos\theta)\sin\omega)^2}{4} + \frac{3(h+2\ell\ \cos\theta)\sin\omega)}{2} + {t_0}^2\right) \\
&\quad + \frac{\sqrt{3}}{48}\frac{E_0(h+2\ell\ \cos\theta)\sin\omega)^3t}{w} \\
y_3b_{22}^{*11} = y_3b_{11}^{*22} &= \frac{2vEt_0}{1-v}\left(\frac{3(h+2\ell\ \cos\theta)\sin\omega)^2}{4} + \frac{3(h+2\ell\ \cos\theta)\sin\omega)}{2} + {t_0}^2\right) \\
&\quad + \frac{\sqrt{3}}{48}\frac{E(h+2\ell\ \cos\theta)\sin\omega)^3t}{vw} \\
y_3b_{12}^{*12} &= \frac{2Gt_0}{\sqrt{3}}\left(\frac{3(h+2\ell\ \cos\theta)\sin\omega)^2}{4} + \frac{3(h+2\ell\ \cos\theta)\sin\omega)}{2} + {t_0}^2\right) \\
&\quad + \frac{\sqrt{3}}{48}\frac{E_0(h+2\ell\cos\theta)\sin\omega)^3t}{w}
\end{aligned}
\tag{60}
$$

To determine the effective elastic properties of the lattice structure, it should be mentioned that the proper cross-sectional areas and also the inertia moments of the cross-sections of each constitutive element of lattice structure (Ω_1 to Ω_{12}) is necessary to consider and investigate [41]. We can determine the homogenized stiffnesses characteristics by considering equation (40) and the elastic properties

of the sandwich shell, where μ, ν takes 0, 1; $k, l, = 1, 2$. For the plate under consideration, coupling stiffness with respect to the virtue of symmetry is equal to zero. The homogenized bending stiffness of the unit cell of I lattice plate is given by $\mu = \nu = 1$ and calculated as

$$K^2_{ijkl} = \left\langle [(-1)^{\nu} y_3^{\nu} b_{22}^{22}(y) + b_{22}^{*22}(y)][(-1)^{\mu} y_3^{\mu}] \right\rangle \tag{61}$$

By substituting the b_{22}^{22} and b_{22}^{*22} in equation (61) and simplifying the equations, we obtain

$$K_{bending,I} = \frac{E_0 {t_0}^2}{1-{\nu_0}^2}((h+2\ell\cos\theta)\sin\omega)\left[\frac{((h+2\ell\ \cos\theta)\sin\omega)^2 {t_0}^2}{2}+1\right] + \frac{2E_0 {t_0}^3}{3(1-{\nu_0}^2)} + \frac{\sqrt{3}}{48}\frac{EH^3 t((h+2\ell\ \cos\theta)\sin\omega)^3}{w} \tag{62}$$

By considering equation (4), we rewrite the stiffness equation by truss fraction factor

$$K_{bending,I} = \frac{E_0 {t_0}^2 \eta}{1-{\nu_0}^2}\left((h+2\ell\cos\theta+b)\sin\omega\left[\frac{((h+2\ell\cos\theta)\sin\omega)^2 {t_0}^2}{2}+1\right] + \frac{2E_0 {t_0}^3}{3(1-{\nu_0}^2)} + \frac{\sqrt{3}}{48}\frac{EH^3 t\eta((h+2\ell\cos\theta+b)\sin\omega)^3}{w}\right. \tag{63}$$

where E_0 and ν_0 are Young's modulus and Poisson's ratio of the plate, E is Young's modulus of the lattice truss structure, t is the thickness of lattice truss, t_0 is the plates thicknesses and H is the height of truss core and h is the height of truss beam. The geometric parameters are shown in Figure 4. Concerning the virtue of symmetry of the plate under consideration, coupling stiffness is equal to zero.

Subsequently, it can be deduced that we can define the effective properties of the lattice structure with respect to use in particular application obtained by changing the geometric parameters such as the face carriers thickness, the core elements parameters like length, cross-sectional areas, the aspect ratio of the shell, the relative height of the core material and the angular orientation of the comprising elements.

Prediction of the lattice strength and peak stress of the I-type core

The macroscopic stress of the unit cell can be expressed as

$$\sigma = \sum_{i=1}^{N} \lambda^{(i)} \sigma^{(i)} n^{(i)} \times n^{(i)} \tag{64}$$

where $\sigma^{(i)}$ is the axial stress of ith truss, and $\lambda^{(i)}$ is its volume ratio. We can calculate the macroscopic collapse stress concerning the kinematically admissible modes of collapse. Hence, we have extracted the equation for the external work to the plastic dissipation associated with the stretching of the trusses [33,42,43]. When all trusses in a unit cell yield in compression or tension simultaneously, the collapse strength σ_{33} is reached and can be determined as

$$\sigma_{33} = \bar{\rho}\eta\sigma_y \sin^2\omega \tag{65}$$

where $\eta = \frac{(h+2\ell cos\theta)}{(h+2\ell cos\theta+b)}$ is the truss mass fraction [33,44]. Considering one strut going through tensile yielding and the opposite strut in compressive yielding, we can determine the out-of-plane shear strengths σ_{33} and σ_{23} in the directions 1 and 2, at collapse stress as follows

$$\sigma_{13} = \bar{\rho}\eta\sigma_y \sin\omega\left(\frac{4\ell\sin\theta\ \sin\omega}{2(h+2\ell\cos\theta)}\right) \tag{66}$$

$$\sigma_{23} = \bar{\rho}\eta\sigma_y \sin\omega\left(\frac{2(h+\ell\sin\theta)\ \cos\omega}{2(h+2\ell\cos\theta)}\right) \tag{67}$$

In this paper the relative density of the structures is low and the unit cell's struts become slender, Hence the peak strength of the structure can be determined by the elastic or plastic bulking [32,43,45,46]. For plastic buckling, the yield stress σ_y can be replaced by the plastic buckling stress σ_c, as follows

$$\sigma_c = \frac{k^2\pi^2 E_t I}{A(h+2\ell\cos\theta)^2} \tag{68}$$

The factor k depends on the rotational stiffness of the nodes and is defined by the conditions of the columns ends; for a pin-joint that can freely rotate $k = 1$ and for built-in joint that does not rotate $k = 2$[42,47,48], A is the cross-sectional area (wt) of the truss, I is the second moment of area of the truss member and E_t is the Shanley-Engesser tangent modulus ($\frac{d\sigma}{d\varepsilon}$), which is determined from the stress versus strain response of the used alloy. The tangent modulus E_t should be replaced by the elastic modulus of the used alloy for calculating the elastic buckling [32,33,48,49]. For I–type lattice structure consisting of strut members having square-shaped cross sections, the plastic buckling stress σ_c is given by

$$\sigma_{c,I} = \frac{k_I{}^2\pi^2 E_t}{12}\left(\frac{t}{0.3(h+2\ell\cos\theta)}\right)^2 \tag{69}$$

where $1 < k_{rotational,I} < 2$. Similarly, for pyramid structures, one has

$$\sigma_{c,p} = \frac{k_p{}^2 \pi^2 E_t}{12} \left(\frac{t}{\ell}\right)^2 \tag{70}$$

where $k_p = 2$.

By replacing the equation (69) into equations (65) and (66), we can define the peak compressive and shear strength for I–type and pyramidal truss structures respectively as

$$\begin{aligned}
\sigma^{pk}_{33,I} &= \frac{\pi^2 \eta}{12\delta} \left(\frac{k_I}{0.33}\right)^2 \sin^3\omega \cos^2\omega \, E_t \bar{\rho}^2 \\
\sigma^{pk}_{13,I} &= \frac{\pi^2 \eta \ell \sin\theta}{6\delta(h + 2\ell\cos\theta)} \left(\frac{k_I}{0.33}\right)^2 \sin^3\omega \cos^2\omega \, E_t \bar{\rho}^2 \\
\sigma^{pk}_{23,I} &= \frac{\pi^2 \eta (h + 2\ell\sin\theta)}{12\delta(h + 2\ell\cos\theta)} \left(\frac{k_I}{0.33}\right)^2 \sin^3\omega \cos 3\omega \, E_t \bar{\rho}^2
\end{aligned} \tag{71}$$

In the same way for the pyramid lattice type structure we have

$$\sigma^{pk}_{33,p} = \frac{\pi^2 \eta}{12\delta} k_p{}^2 \sin^3\omega \cos^2\omega \sin\beta \cos\beta E_t \overline{\rho}^2 \tag{72}$$

$$\sigma^{pk}_{13,p} = \frac{\pi^2 \eta}{12\delta} k_p{}^2 \sin^2\omega \cos^3\omega \sin\beta \cos^2\beta E_t \overline{\rho}^2$$

$$\sigma^{pk}_{23,p} = \frac{\pi^2 \eta}{12\delta} k_p{}^2 \sin^2\omega \cos^3\omega \sin\beta \cos^2\beta E_t \overline{\rho}^2$$

Paying attention to equations (71) and (72) and comparing them for I-type and pyramidal structures, respectively, we have found $(k_{rotational,\ I}/0.33) > k_p$, it means that the I-structure structurally is advantageous over the pyramid structure. Also, it has been seen that the value of $(k_{rotational,\ I}/0.33)$ corresponds mainly to the intersection nodes Q and it is complicated to define it accurately. We have assumed that intersection node Q is fixed at one end and hinged at the other end [13,33,50]. Therefore concerning $(k_{rotational,\ I}/0.33 = 4.92) > k_p$, the I-type structure shows premier properties regarding its capability to resist buckling with a comparison to the pyramidal and X-type structures. The X-type structure mechanical properties have been investigated by Zhanget al. [48,51].

Finite element model, stiffness and strength properties analysis

However, the numerical methods, and the finite element method in particular, represent a very effective tool for solving the unit cell problems

Table 1. The geometric parameters of the I-type lattice cell.

Parameter	Value	Parameter	Value
l	0.005117 m	t	0.0010 m
h	0.01017 m	w	0.0020 m
θ	23.96 degree	ω	66.04 degree
b	0.0030 m	r_1	0.0003 m
r_2	0.00105 m	t_0	0.010 m

and calculating the effective properties. In this section, finite element formulation of the homogenization procedure in Section 2 is derived using 3D solid element.

The commercial software CATIA V5R21 has been used to design the structural models. The geometric parameters of the I-type lattice cell are summarized in Table 1. We used the ABAQUS software to verify and analyze the finite element models for pyramidal, X-type and I-type lattice structures. The compression and shear tests models have simulated and investigated with a focus on the unit solutions to find the effective stiffness and effective strength. Consequently, the truss-wall models are based on the solid-wall models shown in Figure 2. The lattice plate model is made of the main homogenized equivalent core and two solid-face sheets, with geometrical parameters equal to those used in experimental measurements [48].

First, concerning the solution of the unit cell equations (29)–(31), Where w_1 and w_2 determine the ratio of the in-plane to thickness dimensions of the unit cell. In the particular structure, these ratios are constants. Equations (29)–(31) are very similar in form with the equilibrium and constitutive equations in the theory of elasticity, except for the terms C_{ijkl} and $y_3 C_{ijkl}$ in equation (29). We discretize the unit cell with the solid finite element similar to the variation procedure of elastic problem in finite element theory [52], hence the following finite element formulation of equations (30) and (31) can be drawn easily

$$\begin{aligned} Ka^{kl} &= f^{kl} \\ Ka^{*kl} &= f^{*kl} \\ K &= \int_{\Omega} B^T c B \mathrm{d}\Omega \\ K^{kl} &= \int_{\Omega} B^T c \varepsilon^{0(kl)} \mathrm{d}\Omega \\ K^{*kl} &= \int_{\Omega} z B^T c \varepsilon^{0(kl)} \mathrm{d}\Omega \end{aligned} \tag{73}$$

where K is global stiffness matrix, f^{kl}, f^{*kl} are global nodal force vectors, a^{kl}, a^{*kl} are global nodal displacement vectors. The local functions U, and V are related to

the a^{kl} and a^{*kl}, respectively. The strain-displacement matrix is B, the elasticity matrix is c . To calculate the integrations on the unit cell, the summation of element-wise quantities is applied. Superscript kl denotes load cases $kl \in \{11, 22, 12\}$. Hence there are six load cases in all, corresponding to six unit strain vectors $\varepsilon^{0(kl)}$ and $z\varepsilon^{0(kl)}$. The finite element formulation of equation (29) is

$$\begin{aligned} b^{kl} &= c(\varepsilon^{0(kl)} - \varepsilon^{kl}) \\ b^{*kl} &= c(z\varepsilon^{0(kl)} - \varepsilon^{*kl}) \end{aligned} \tag{74}$$

The effective stiffness coefficients are got by average on the b^{kl} and b^{*kl}. The numerical implementation procedure of periodic plate structure is described as follows. Firstly, the finite element model of the unit cell has been constructed in Abaqus software. In next step, the nodal displacement of the finite element model has been applied concerning to equivalent unit strain fields. The unit strain fields include three in-plane $\varepsilon^{0(kl)}$ and three flexural strain fields $z\varepsilon^{0(kl)}$. Their nodal force vector can be calculated by multiplying stiffness matrix K with the displacement field as

$$\begin{aligned} f^{kl} &= K\chi^{0(kl)} \\ f^{*kl} &= K\chi^{*(kl)} \end{aligned} \tag{75}$$

where $\chi^{0(kl)}$ and $\chi^{*(kl)}$ are nodal displacement vectors. In Abaqus software, we can just apply nodal displacement vectors $\chi^{0(kl)}$ and $\chi^{*(kl)}$ on each node. We can define nodal reaction force f^{kl} or f^{*kl} by run one static analysis, and get them directly from software's output. Here K, f^{kl} and f^{*kl} are stiffness matrix and force vector without periodic boundary conditions. The force vector is applied to nodes in the unit cell by calculation of equivalent nodal force vectors in equation (75). Subsequently, the finite element equations (73) under periodic boundary conditions have solved.

It should be mentioned that here periodicity of the plate is in-plane, and the top and bottom face boundaries are free.

The Abaqus software capability is only to apply nodal force f^{kl} and f^{*kl} on each node, apply periodic boundary conditions, perform static analysis, and define characteristic displacement field a^{kl} and a^{*kl}. So after the characteristic displacement fields a^{kl} and a^{*kl} are obtained, the effective stiffness coefficients are defined in the unit cell. To calculate the stiffness matrix K of the unit cell in Abaqus software, we applied the characteristic displacement field a^{kl} and a^{*kl} on every node, performed static analysis, and got corresponding nodal reaction force. In brief, the whole process has mainly consisted of parts: 1. Define equivalent nodal force vector, equation (75). 2. Define characteristic displacements by solving equilibrium equations. 3. Define the effective modulus by using the characteristic displacements.

The lattice truss structures were simulated by using expanded AISI 304 stainless steel sheets, with 21 mm in length, 30 mm in width and 14 mm in height for the core and 2 mm in thickness for the face sheets. The applied material, AISI304 stainless steel, has a density of 8 kg/cm^3, Young's modulus of 200 GPa, Poisson's ratio of 0.29, initial yielding strength of 215 MPa, and ultimate strength of 505 MPa [13]. The equivalent elastic constants were used for the homogenized core simulation procedure and the appropriate elastic tensor of material is calculated in appendix A. It has been established that the three lattice structures have the same equivalent elastic constants, given by

$$\begin{bmatrix} C_{11} & C_{12} & C_{13} & 0 & 0 & C_{16} \\ C_{12} & C_{22} & C_{23} & 0 & 0 & C_{26} \\ C_{13} & C_{23} & C_{33} & 0 & 0 & C_{36} \\ 0 & 0 & 0 & C_{44} & C_{45} & 0 \\ 0 & 0 & 0 & C_{45} & C_{55} & 0 \\ C_{16} & C_{26} & C_{36} & 0 & 0 & C_{66} \end{bmatrix} = \begin{bmatrix} 0.227 & 0.349 & 0.528 & 0 & 0 & 0 \\ 0.351 & 0.601 & 0.868 & 0 & 0 & 0 \\ 0.581 & 0.911 & 1.349 & 0 & 0 & 0 \\ 0 & 0 & 0 & 0.392 & 0 & 0 \\ 0 & 0 & 0 & 0 & 0.941 & 0 \\ 0 & 0 & 0 & 0 & 0 & 0.586 \end{bmatrix} \times 10^3 MPa \tag{76}$$

The loading faces were bonded to rigid plates and the boundary condition on them were considered unable to rotate or displace laterally, such that the bonded surfaces of the nodes. To impose the periodic boundary conditions on all lateral surfaces of the model, we considered that the displacements of the nodes on both surfaces of the structure are same. The compression and shear FE simulations followed the ASTM C 365–00 and ASTM C 237–00 guidelines, respectively. Compression simulates with considering a nominal strain rate of $1 \times 10^{-3} s^{-1}$ and shear simulates with considering a nominal strain rate of $1 \times 10^{-4} s^{-1}$. The dimensions of the expanded three types of lattice truss core structures with the predicted relative density and truss mass fraction are listed in Table 2.

For the pyramidal lattice, the mesh size is 0.2, the applied mesh type is a tetrahedron called C3D4. Also, the total number of nodes and elements are 4,95,326, and 2,79,246 respectively and has used to the model of constituent lattice face

Table 2. Dimensions of the expanded lattice structures with the predicted and post brazed measured relative density.

	Truss measurements					Relative density		
Lattice structure	Width (m)	Thickness (m)	Length (m)	Brazed length (m)	Coefficient η	Predicted numerical	Measured FEM	Measured experiments
Pyramid	0.002	0.001	0.022	0.003	0.78	0.0195	0.0204	0.021
X-Type	0.002	0.001	0.022	0.003	0.81	0.0176	0.0192	0.0183
I-Type	0.002	0.001	0.022	0.003	0.86	0.0165	0.181	–

sheets, struts members, and the face sheets. For the x-type lattice, the mesh size is 0.2, the applied mesh type is a tetrahedron called C3D4, the total number of nodes is 5,43,287 and the total number of elements is 2,99,871. For the I-type lattice, the mesh size is 0.2, the total number of nodes is 5,75,693 and the total number of elements is 3,21,873. The applied mesh type is also the tetrahedron called C3D4. It uses the static analysis by ABAQUS standard.

We have established the different set of FE models to validate the homogenization model and to compare with the numerical and experimental measurements for X-type and I-type lattice plate structures. We used the stress versus strain curve and assumed the solid material follow the Mises yield criterion to determine uniaxial response characteristic of structures. The numerical and FE-simulated stress versus strain curves of the three types of lattice structures, subjected to strength and shear compression separately, are plotted in Figure 7. Subsequently, more detailed information on a comparison of the predicted elastic moduli and peak strengths with numerical and FE simulation measurements are listed in Table 3 and compared with the results of validated experimental results by Zhang et al. [48,51].

Considering both compression and shear loads caused by clamping forces, we should design the core elements with well-recognized regulation for vehicle braking systems, ECE R13-H. According to an international regulation ECE R13-H, the compressive stress applied by the brake actuators and brake pads should be estimated to be up to 1.5 MPa and also the shear stress should be 1.2 MPa for a typical passenger vehicle with a weight of 1.5 tons. So, the core elements designed in the ventilated brake disc should be stiff enough and have proper heat-removal capability.

The compressive peak strengths predicted by the numerical model and the 3D FE model are in good agreement with the experimental measurements. The 3D FE predictions of the compressive peak stresses are 1.3 MPa, 1.639 MPa and 1.66 MPa for the pyramidal, X-type and I-structures, respectively; the numerical predictions are 1.33 MPa, 1.83 MPa and 1.94 MPa; the corresponding experimental results for pyramidal and X-type are 1.28 MPa, 1.635 MPa. By comparing the numerical and

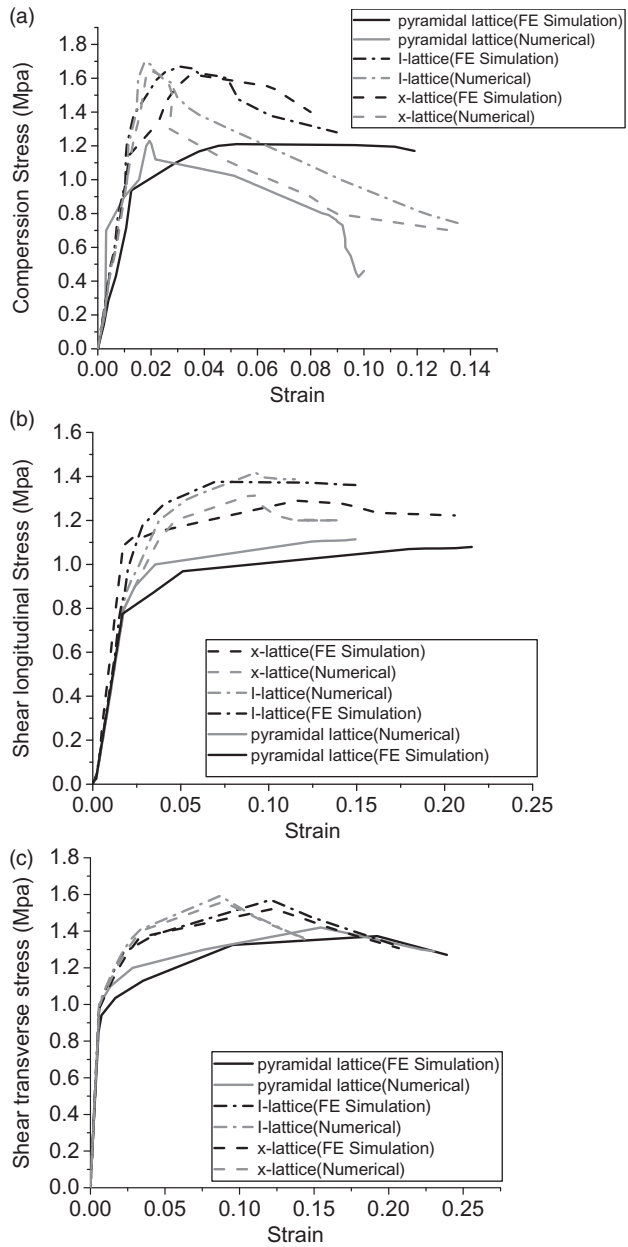

Figure 7. Stress versus strain curves of three types of lattice plate structures with modified predictions of FE simulation and numerical measurements: (a) Out-of-plane compression; (b) shear in longitudinal direction; (c) shear in transverse direction.

Table 3. Summary of Simulated and numerical results of non-dimensional stiffness and mechanical properties of lattice structures.

Non- dimensional properties		Compressive modulus (MPa)	Compressive strength (MPa)	Shear modulus (MPa)		Shear strength (MPa)	
				Longitudinal (G_{13})	Transverse (G_{23})	Longitudinal (σ_{13})	Transverse (σ_{23})
Numerical results	Pyramidal	642	1.33	286	602	1.12	1.31
	X lattice	651	1.83	315	617	1.41	1.38
	I lattice	663	1.94	328	631	1.56	1.46
FE Simulation results	Pyramidal	604	1.32	298	586	1.09	1.46
	X lattice	637	1.639	328	603	1.28	1.50
	I lattice	659	1.667	344	615	1.41	1.53
Test results	Pyramidal	561	1.28	292	501	0.94	1.21
	X lattice	578	1.635	314	530	1.25	1.28

FE simulation predictions with validated experiments, the value of k for the I-type lattice can be inferred to be $k_{bending,\ I} = 1.506$ for the bending stiffness concerning the equation (63). Also, for the rotational stiffness can infer to be k = 4.92 and the simulated compressive value was substituted into equation (70) to calculate stiffness. The results of Figure 7 and Table 3 demonstrate that the I-structure has a significantly greater plastic buckling resistance than the pyramidal and X-type lattice structures does. In general, the I-type structure is superior to the other two types of lattice structures in terms of the mechanical strength. On the other hand with paying attention to Table 3 and Figure 7 and concerning the truss mass fraction factor (η), By increasing (η) the mechanical strength of lattice and the stiffness of lattice plate structures increase as for I-type lattice is more than X-type and pyramidal lattice respectively. The stress versus strain curves of three type of lattice plate structures are as follows:

Accordingly, it can be defined from Table 3 and Figure 7 that the numerical predictions of the elastic moduli properties of all type of structures are notably greater than those measured in FE simulations and experimental tests. As an example, the numerical and FE-simulated results predicted compressive moduli of the I-type structure are 663 MPa and 659 MPa, respectively. The deviation of moduli and peak strengths in FE simulations data and numerical predictions with test measured data are mainly due to various processing method-induced defects in real structures and has a notable effect in degrading the elastic stiffness rather than the strength of cellular metals [13,53,54]. Therefore, we consider ideal structures that have no defect and were simulated in the present study. Hence, the effects of various defects such as micro-cracks existing in strut members and intersection nodes, different sizes of strut element and node area, and a non-rectangular cross-section of strut member on stiffness and strength are considerable which are

related to the geometrical imperfection of trusses and node areas. Even so, the results of Table 3 represent that the numerical measurements predicted compressive and shear moduli are close to the corresponding FE predictions (the maximum deviation less than 8%) and experimental tests done by Zhang et al. [48].

On the braking application point of view, a variation of stiffness and strength of brake disc have an important effect on the contact stiffness, used to put out the adaptability between the contact surfaces to define the realistic contact behavior. If the contact stiffness goes to $K_{Contact} = \infty$, there is no penetration and is the ideal condition. Actually, to achieve small acceptable contact penetration, a high-enough stiffness is necessary. On the other hand, the unreasonable relative displacement between the two contact surfaces and excessive penetration of one surface into the other causes too weak a contact stiffness. An appropriate value of contact stiffness can be determined by carrying out numerical trials over a range of stiffness. So we put forward the feasibility of the numerical measurements and hence the homogenization technique developed in the present study especially for the lattice plate structures in various applications such as in brake disc designs.

Conclusion

The paper develops the micro-mechanical model for periodic composite sandwich structure by considering the modified two-scale asymptotic homogenization method. The method applies to the 3D elastic problem of inhomogeneous composite structure built of orthotropic material. The special type of elasticity problem concerning periodicity boundary conditions and considering some variables are used to represent the I lattice sandwich structure problem. Numerical solution of a cellular problem to define the mechanical properties of lattice plate is related to the parameters: the periodicity boundary conditions, the type and geometry of periodicity cell Y, the material characteristics $C_{ijkl}(y)$, the boundary conditions, the periodicity conditions with a suitable function.

The peak strength and the stiffness of lattice plate structures have been shown to depend upon the six factors. It creates a desirable way to define the proper contact stiffness and strength of lattice design. The factors are: (i) the stress–strain response of the parent alloy, (ii) the truss mass fraction coefficient (η), (iii) the relative density (ρ), (iv) the thickness, Young's modulus and Poisson ratio of the face carrier plates and truss core structure, (v) the geometric of the truss core and (vi) The inner nodes of the cellular structure concerning satisfying rigid-joint conditions and connecting to the plate surfaces.

Stiffness and strength of lattice plate structures are related to the truss mass fraction coefficient (η) and are decreased by the truss mass fraction coefficient as for the pyramidal lattice reduced from that of X-type and I-type lattices. Also, strength has good agreement with those of modified prediction of the simulation and experimental results.

The measured compressive strength and shear strength in both longitudinal and transverse conditions are also found to be in reasonable agreement with the

modified predictions of FE simulation and numerical measurements. The I-type lattice has shown the superior mechanical properties, providing approximately 7% higher peak compressive, 10% shear longitudinal strength and 3% shear transverse strength for a given relative density, stiffness and truss fraction.

Declaration of conflicting interests

The author(s) declared no potential conflicts of interest with respect to the research, authorship, and/or publication of this article.

Funding

The author(s) disclosed receipt of the following financial support for the research, authorship, and/or publication of this article: The paper was supported by the national natural science foundation of china (grant number 51675281) and fundamental research funds for the central universities of china (grant number 30916011302).

References

1. Dunlap KB, Riehle MA and Longhouse RE. An investigative overview of automotive disc brake noise. *SAE International*. 1999
2. Ouyang H, Nack W, Yuan Y, et al. Numerical analysis of automotive disc brake squeal: a review. *Ijvnv*. 2005; 1: 207–231.
3. Thomas TH. Disc Brakes "Two Years After. *SAE International*. 1967;
4. Limpert R. Brake design and safety. 2011.
5. Palmer E, Mishra R, Fieldhouse J, et al. Analysis of Air Flow and Heat Dissipation from a High Performance GT Car Front Brake. *SAE International*. 2008; ■.
6. Pevec M, Potrc I, Bombek G, et al. Prediction of the cooling factors of a vehicle brake disc and its influence on the results of a thermal numerical simulation. *Int J Automot Technol*. 2012; 13: 725–733.
7. Mackin TJ, Noe SC, Ball KJ, et al. Thermal cracking in disc brakes. *Eng Failure Anal*. 2002; 9: 63–76.
8. Nejat A, Aslani M, Mirzakhalili E, et al. Heat transfer enhancement in ventilated brake disk using double airfoil vanes. *J Thermal Sci Eng Appl*. 2011; 3: 045001–045010.
9. Anoop S, Natarajan S and Kumaresh Babu SP. Analysis of factors influencing dry sliding wear behaviour of Al/SiCp–brake pad tribosystem. *Mater Design*. 2009; 30: 3831–3838.
10. Gao CH, Huang JM, Lin XZ, et al. Stress analysis of thermal fatigue fracture of brake disks based on thermomechanical coupling. *J Tribol*. 2006; 129: 536–543.
11. Phan D and Kondyles D. Rotor design and analysis; a technique using computational fluid dynamics (CFD) and heat transfer analysis. *SAE International*. 2003;
12. Shen Y, Mckown S, Tsopanos S, et al. The mechanical properties of sandwich structures based on metal lattice architectures. *J Sandwich StructMater*. 2010; 12: 159–180.
13. Wadley HNG. Multifunctional periodic cellular metals. *Philos Trans A Math Phys Eng Sci*. 2006; 364: 31–68.
14. Deshpande VS, Fleck NA and Ashby MF. Effective properties of the octet-truss lattice material. *J Mech Phys Solids*. 2001; 49: 1747–1769.

15. Kılıçaslan C, Odacı İK and Güden M. Single- and double-layer aluminum corrugated core sandwiches under quasi-static and dynamic loadings. *J Sandwich Struct Mater*. 2016; 18: 667–692.
16. Wallach JC and Gibson LJ. Mechanical behavior of a three-dimensional truss material. *Int J Solids Struct*. 2001; 38: 7181–7196.
17. Wang AJ and McDowell DL. In-plane stiffness and yield strength of periodic metal honeycombs. *J Eng Mater Technol*. 2004; 126: 137–156.
18. Yan HB, Zhang QC and Lu TJ. An X-type lattice cored ventilated brake disc with enhanced cooling performance. *Int J Heat Mass Transfer*. 2015; 80: 458–468.
19. Atas C and Potoğlu U. The effect of face-sheet thickness on low-velocity impact response of sandwich composites with foam cores. *J Sandwich Struct Mater*. 2016; 18: 215–228.
20. Gunes R, Arslan K, Apalak MK, et al. Ballistic performance of honeycomb sandwich structures reinforced by functionally graded face plates. *J Sandwich Struct Mater*. 0: 1099636216689462;
21. Karamoozian A, Tan CA, Wang L, et al. Sensitivity analysis of the equal angle divider mechanism kinematics with synthesis of the joint gap tolerances. *Mechanics Based Design of Structures and Machines*. 2017;
22. Francfort GA and Murat F. Homogenization and optimal bounds in linear elasticity. *Arch Rational Mech Anal*. 1986; 94: 307–334.
23. Milton GW and Kohn RV. Variational bounds on the effective moduli of anisotropic composites. *J Mech Phys Solids*. 1988; 36: 597–629.
24. Kalamkarov A. The thermal conductivity of a twisted nonuniform anisotropic layer of periodic structure with wavy surfaces. *JEP*. 1987; 52.
25. Kalamkarov AL. The thermoelasticity problem for structurally nonuniform shells of regular structure. *J Appl Mech Technical Phys*. 1989; 30: 981–988.
26. Kalamkarov AL and Kolpakov AG. Analysis, design, and optimization of composite structures. 1997.
27. Ptochos E and Labeas G. Elastic modulus and Poisson's ratio determination of micro-lattice cellular structures by analytical, numerical and homogenisation methods. *J Sandwich Struct Mater*. 2012; 14: 597–626.
28. Kolpakov AG. Variational principles for stiffnesses of a non-homogeneous plate. *J Mech Phys Solids*. 1999; 47: 2075–2092.
29. Mai SP. Experiment on box-section sandwich beams in three-point bending. *J Sandwich Struct Mater*. 2014; 16: 534–550.
30. Wicks N and Hutchinson JW. Optimal truss plates. *Int J Solids Struct*. 2001; 38: 5165–5183.
31. Bitzer T. *Honeycomb technology: materials, design, manufacturing, applications and testing*. London, New York: Chapman & Hall, 1997.
32. Queheillalt DT and Wadley HNG. Pyramidal lattice truss structures with hollow trusses. *Mater Sci Eng A*. 2005; 397: 132–137.
33. Kooistra GW and Wadley HNG. Lattice truss structures from expanded metal sheet. *Mater Design*. 2007; 28: 507–514.
34. Wu X and Ohno NA. Homogenization theory for inelastic behavior of materials with periodic internal structures. In: *IUTAM symposium on micro- and macrostructural aspects of thermoplasticity: Proceedings of the IUTAM symposium* (eds Bruhns OT and Stein E), Bochum, Germany, 25–29 August 1997, pp.187-196, Dordrecht: Springer Netherlands, 2002.

35. Noor AK. Continuum modeling for repetitive lattice structures. *Appl Mech Rev*. 1988; 41: 285–296.
36. Kolpakov AG. Application of homogenization method to justification of 1-D model for beam of periodic structure having initial stresses. *Int J Solids Struct*. 1998; 35: 2847–2859.
37. Kolpakov AG. Variational principles for stiffnesses of a non-homogeneous beam. *J Mech Phys Solids*. 1998; 46: 1039–1053.
38. Saha GC, Kalamkarov AL and Georgiades AV. Effective elastic characteristics of honeycomb sandwich composite shells made of generally orthotropic materials. *Compos A Appl Sci Manuf*. 2007; 38: 1533–1546.
39. Kolpakov AG. Application of the averaging method in the calculation of rod structures like plates and beams. *J Appl Mech Tech Phys*. 1998; 39: 801–809.
40. Kalamkarov AL and Challagulla KS. Effective properties of composite materials, reinforced structures and smart composites: asymptotic homogenization approach. In: M Kachanov and I Sevostianov (eds) *Effective properties of heterogeneous materials*. Dordrecht: Springer Netherlands, 2013, pp.283–363.
41. Kalamkarov AL and Georgiades AV. Micromechanical modeling of smart composite structures. *Smart Mater Struct*. 2002; 11: 423
42. Vigliotti A and Pasini D. Structural optimization of lattice materials. 2011: 925–934.
43. Zhang G, Wang B, Ma L, et al. Response of sandwich structures with pyramidal truss cores under the compression and impact loading. *Compos Struct*. 2013; 100: 451–463.
44. Vigliotti A and Pasini D. Stiffness and strength of tridimensional periodic lattices. *Comput Meth Appl Mech Eng*. 2012; 229–232: 27–43.
45. Rejab MRM and Cantwell WJ. The mechanical behaviour of corrugated-core sandwich panels. *Compos Part B: Eng*. 2013; 47: 267–277.
46. Dahiwale N, Panigrahi S and Akella K. Numerical analyses of sandwich panels with triangular core subjected to impact loading. *J Sandwich Struct Mater*. 2015; 17: 238–257.
47. Choi J, Lee J, Lee J-H. Development of ideal solution and validation of stiffness and strength by finite element method for truss-wall corrugated cellular solids. *J Mech Sci Technol*. 2014; 28: 1765–1778.
48. Zhang Q, Han Y, Chen C, et al. Ultralight X-type lattice sandwich structure (I): Concept, fabrication and experimental characterization. *Sci China Ser E-Technol Sci*. 2009; 52: 2147–2154.
49. Gümrük R and Mines RAW. Compressive behaviour of stainless steel micro-lattice structures. *Int J Mech Sci*. 2013; 68: 125–139.
50. Jeong J, Lee Y and Cho M. Sequential multiscale analysis on size-dependent mechanical behavior of micro/nano-sized honeycomb structures. *Mech Mater*. 2013; 57: 109–133.
51. Zhang Q, Chen A, Chen C, et al. Ultralight X-type lattice sandwich structure (II): Micromechanics modeling and finite element analysis. *Sci China Ser E-Technol Sci*. 2009; 52: 2670–2680.
52. Cai Y, Xu L and Cheng G. Novel numerical implementation of asymptotic homogenization method for periodic plate structures. *Int J Solids Struct*. 2014; 51: 284–292.
53. Chen C, Lu TJ and Fleck NA. Effect of imperfections on the yielding of two-dimensional foams. *J Mech Phys Solids*. 1999; 47: 2235–2272.
54. Schaedler TA, Jacobsen AJ, Torrents A, et al. Ultralight metallic microlattices. *Science*. 2011; 334: 962–965.

55. Kalamkarov AL. *Composite and reinforced elements of constructions*. West Sussex, UK: John Wiley & Sons Ltd, 1992, p.286.
56. Reddy JN. *Mechanics of laminated composite plates- theory and analysis(book)*. Boca Raton, FL: CRC Press, 1997.

Appendix

Nomenclature

a^{kl}	the global nodal displacement vectors
a^{*kl}	the global nodal displacement vectors
b	brazed node width area [m^2]
b_{il}^{kl}	coefficient of local structure stress field
b_{il}^{*kl}	coefficient of local structure stress field
C_{ijkl}	tensor of local elastic constants of the body
e_{kl}	strain tensor
f^{kl}	global nodal force vectors
f^{*kl}	global nodal force vectors
G	occupied region by the composite
h	height of truss beam [m]
H	the height of truss core [m]
k	factor depends on the rotational stiffness of the nodes
k_l	the factor of rotational stiffness for I-type lattice
k_p	factor of rotational stiffness for I-type lattice
K_{ijkl}^0	in-plane stiffness
K_{ijkl}^1	coupling stiffness
K_{ijkl}^2	bending stiffness
$K_{ijkl}^{\nu+\mu}$	the plate stiffness
ℓ	strut length [m]
L_ε	elasticity theory operator
m	the total number of nodes
n	normal to the free surface
Oy_1	orientation
Oy_2	coordinate orientation
Oy_3	orientation
Oy_1'	orientation
Oy_2'	orientation
Oy_3'	coordinate orientation

S	the projection of Y on the Oy_1y_2 plane
t	thickness of lattice truss shell [m]
t_0	plate's thicknesses [m]
u^ε	displacements$u(y)$ =periodic displacement function in y_1, y_2 with periodicity cell T
U_k^{kl}	homogenized periodicity cell local function
V_k^{kl}	homogenized periodicity cell local function
V_U	with respect to unit cell [m^3]
V_T	total volume of the solid metal within the unit cell [m^3]
W	truss width [m]
$w_1,\ w_2$	ratios of the tangential dimensions of the shell to the thickness
$X_{k,1}^{\nu kl}(y)$	periodic displacement function in y_1, y_2 with periodicity cell T
δ	dimensionless parameter and defines the thickness of the shell
ε	small parameter characterizing dimension of a unit cell Y, dimensionless
εY	of small dimensions of periodicity cell
η	truss fraction factor
θ	the inclination angle between the truss members [°]
λ	that related to the unit cell volume
$\lambda^{(i)}$	ratio
$\bar{\rho}$	the relative density
σ_c	plastic buckling stress [MPa]
σ_y	yield stress [MPa]
$\sigma^{(i)}$	axial stress of the ith truss [MPa]
σ_{ij}^ε	stresses tensor
σ_{12}	out-of-plane shear strength in longitudinal direction [MPa]
σ_{23}	out-of-plane shear strength in transverse direction [MPa]
σ_{33}	the collapse strength
τ	torsional and flexural torsional strains of the middle surface
$\chi^{0(kl)}$	nodal displacement vectors
$\chi^{*(kl)}$	the nodal displacement vectors
ω	the inclination angle between truss member and the base of the unit cell [°]
Ω_δ	periodicity cell

Appendix 1

It should be mentioned that the global coordinates have been used to govern differential equations and associated surface boundary conditions of the unit-cell problems for a rotated element of the lattice structure. However, the final expressions in equation (60) could be defined by the familiar material constants

(Young's moduli, shear moduli, and Poisson's ratios). So the off-axis coefficients, C_{ijkl}, should be related with the principal material coefficients, $C^{(m)}_{jkl}$. To do this, the tensor transformation equation for a fourth-order tensor has to be applied.

$$C_{ijkl} = a_i a_j a_k a_l C^{(m)}_{ijkl} \tag{77}$$

Equation (77) has expanded for an orthotropic material and consequently, the principal material coefficients, $C^{(m)}_{jkl}$, are related to the material constants, E_1, E_2, G_{12}, υ_{12}, etc. ([55,56]).